EFFECT OF COOLING PROCESS ON POROSITY IN THE ALUMINUM ALLOY AUTOMOTIVE WHEEL DURING LOW-PRESSURE DIE CASTING

Dashan Sui and Zhenshan Cui
National Die and Mold CAD Engineering Research Center, Shanghai Jiao Tong University, Shanghai, China

Rong Wang and Shengfei Hao
Department of Technology Development, Dare Wheel Manufacturing Co., Ltd., Zhenjiang, Jiangsu, China

Qingyou Han
Department of Mechanical Engineering Technology, Purdue University, West Lafayette, IN, USA

DOI 10.1007/s40962-015-0008-0

Abstract

Experiments were conducted to verify the feasibility of cooling process for one aluminum alloy wheel during low-pressure die casting, and the results showed there were some macroporosity defects in the junctions of small spokes. Numerical simulation was implemented, and the rational cooling and insulation process was determined by analyzing the solidification times of different stages at some locations of casting. The simulation and experimental results both demonstrated the insulation spots had a good effect on prolonging solidification time at the location with thin wall thickness, preventing the feeding paths cutoff prematurely and decreasing the size of porosity defects distinctly.

Keywords: *aluminum alloy wheel, low-pressure die casting, numerical simulation, cooling process, porosity*

Introduction

Energy saving and emission reduction are priority objectives of international policies. The automotive industry is moving toward an increased usage of light alloy castings. As one of critical components, aluminum alloy wheels offer improved aesthetic appearance and design flexibility over the traditional stamped and welded steel products.[1] Low-pressure die casting (LPDC) is a popular process for making aluminum alloy wheels, since it has many advantages, such as stable filling, short product cycles, and near-net-shape forming and is easily molded into intricate shapes.

The LPDC process of aluminum alloy wheel has been studied quite intensively. Kuo et al.[2] developed an interactive computer simulation system to aid the determination of the pressure–time relationship for the LPDC process to eliminate filling-related defects while maintaining its productivity. Hines[3] researched the determination of the interfacial heat transfer boundary conditions in an aluminum low-pressure permanent mold test casting. Zhang et al.[4] studied the casting defects of aluminum alloy wheels in the LPDC process. Miller et al.[5] investigated the erosive–corrosive wear of aluminum A356 during the LPDC process. Zhang et al.[6] developed a 3D thermal model of the LPDC process for A356 aluminum alloy wheels. Zhang et al.[7] optimized the process parameters of the LPDC process with soft computing. Maijer et al.[8] investigated the predictive control for aluminum wheel casting via a virtual process model. Mi et al.[9] studied the numerical simulation of a LPDC aluminum wheel. Cleary[10] researched the feeding, freezing and defects creation during the LPDC process by using smoothed particle hydrodynamics mesh-free Lagrangian method. Shi et al.[11] investigated the determination of the optimal location to monitor temperature during the LPDC process. Reilly et al.[12] developed the process modeling of aluminum alloy automotive wheels for the LPDC process.

Porosity, as one of the LPDC process minimizing defects, is a continuing production challenge since it is the main source of rejected castings due to their deleterious effects on the mechanical properties and surface quality.[13–15] The

Published online: 30 November 2015

reduction in the porosity formation can promote sequential solidification and eliminate hot spots in castings.[11]

The development and application of numerical simulation technology in the foundry is playing an important role for designing and optimizing the casting parameters. In this paper, numerical simulation was implemented to study the effect of the cooling process on the porosity of an aluminum alloy wheel during LPDC. Figure 1 shows the model and its section. The wheel had five big spokes and five small spokes. Hot spots were easily formed in the junctions during solidification which could cause porosity defects. Thus, the characteristics of solidification were investigated by simulation, and rational cooling process was determined to promote sequential solidification and avoid porosity defects. Finally, the experiments were conducted to verify the feasibility of the improved cooling and insulation process.

Experimental Procedure

LPDC experiments were conducted to verify the feasibility of the cooling process for the wheel, and the assembly of the LPDC process is shown in Figure 2. The aluminum alloy A356 was used for producing the casting, and the pouring temperature was 685 °C (1265 °F). The top die, side die and bottom die were all preheated to 350 °C (662 °F). The pressure curve is shown in Figure 3, in which the pressure began to release when solidification completed. It is clear that the time of pressure release varied with the different cooling process.

Initial Cooling Process

Some cooling spots were designed on the top and bottom die. The cooling spots on the top die are shown in Figure 4. The C1 location was water-cooled, and C2–C26 locations were air-cooled. C2–C6, C7–C16 and C17–C26 belonged to the same group, respectively, which could be switched on/off at the same time. The cooling spots on the bottom die are shown in Figure 5. All spots were air-cooled. C27–C31 and C32–C36 belonged to the same group separately.

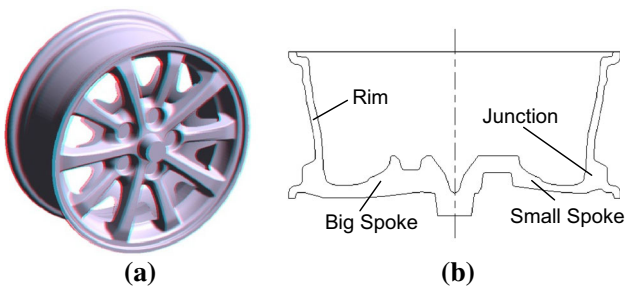

Figure 1. Aluminum alloy wheel model. (a) CAD model, (b) sectional drawing.

The times of switch on/off the cooling spots are defined and listed in Table 1.

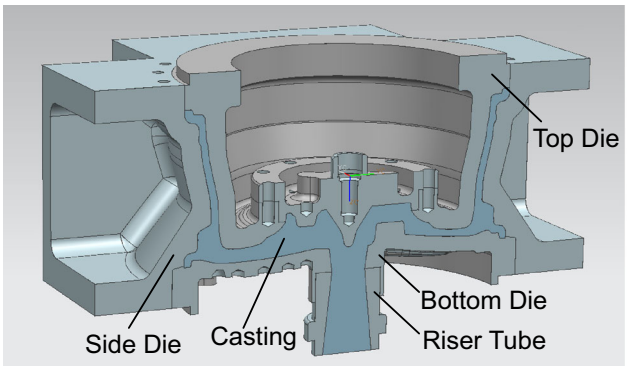

Figure 2. Assembly of LPDC process.

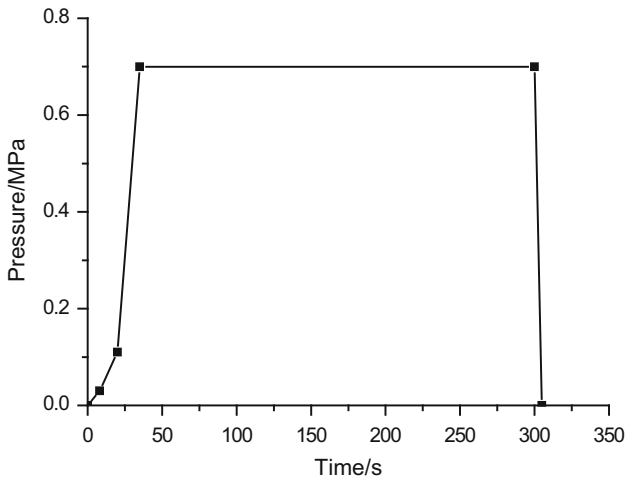

Figure 3. Pressure curve.

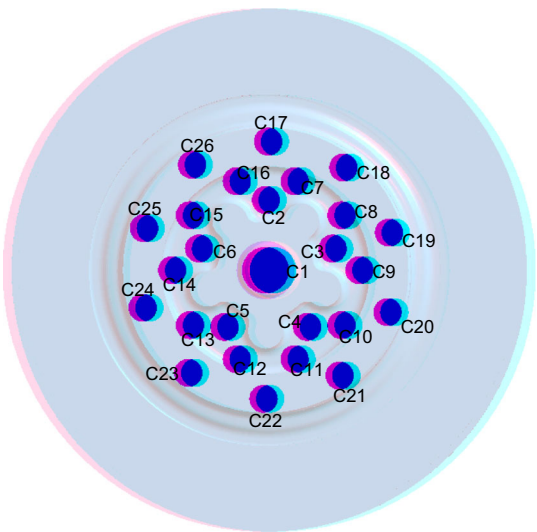

Figure 4. Cooling spots on top die.

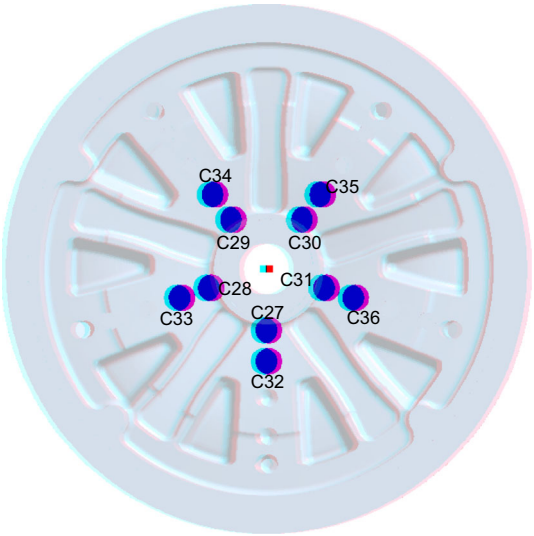

Figure 5. Cooling spots on bottom die.

Table 1. Time of Switch On/Off of Cooling Spots

No. of spots	Time of switch on (s)	Time of switch off (s)
C1	170	50
C2–C6	140	220
C7–C16	130	260
C17–C26	190	220
C27–C31	110	260
C32–C36	200	260

Temperature Measurement

The K-type thermocouples were used to measure the temperature of the dies, with a response time of 0.5 s. One thermocouple (TC1) was placed in the side die, and the other one (TC2) was fixed in the bottom die, as shown in Figure 6, and the measured temperature curves could be obtained.

Porosity Defects

LPDC experiments were conducted for about 100 cycles. One of the experimental wheel castings is shown in Figure 7. Each casting must be tested by X-ray inspection equipment to detect whether there are porosity defects. The test results indicated most castings had some macroporosity defects in the junctions. The defects were about grade 4 in small spokes and grade 2 in big spokes according to the standard ASTM E 155, illustrated in Figure 8. Consequently, the casting was cut and is shown in Figure 9. The physical size of macroporosity in the small spoke is about 5.5 mm, while there was no macroporosity in the big spoke. However, the technical requirement of

Figure 6. Thermocouple location.

Figure 7. Wheel casting.

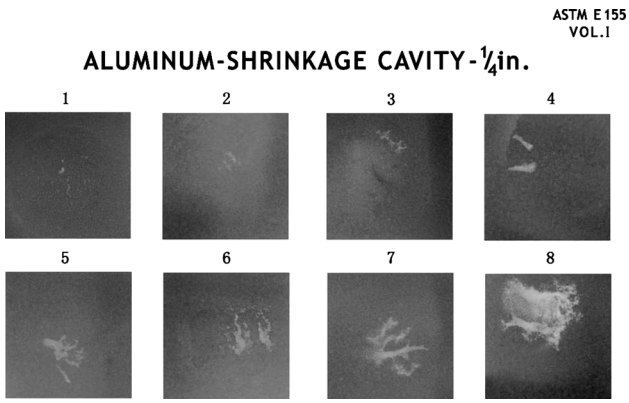

Figure 8. X-ray inspection standard.

macroporosity must be less than grade 3 which meant the casting was unqualified and the cooling process should be improved to avoid the defects.

Simulation Modeling

MAGMA version 5.2 software, with its module-MAGMAlpdc, was used for numerically simulating the filling and solidification behavior of the wheel casting. Solidification times of different stages and porosity criterions were analyzed and compared with experimental results.

Figure 9. Macroporosity defects.

Moreover, the cooling process was improved to avoid the formation of porosity defects.

Governing Equations

Basic governing equations of filling simulation include mass equation, momentum equation and energy equation, and the expressions are as follows.[16,17]

Mass conservation equation:

$$\frac{\partial \rho}{\partial t} + \nabla \cdot (\rho \mathbf{u}) = 0 \qquad \text{Eqn. 1}$$

Momentum conservation equation:

$$\frac{\partial (\rho u)}{\partial t} + \nabla \cdot (\rho u \mathbf{u}) = \nabla \cdot (\mu \cdot \text{grad} u) - \frac{\partial p}{\partial x} + S_u \qquad \text{Eqn. 2}$$

$$\frac{\partial (\rho v)}{\partial t} + \nabla \cdot (\rho v \mathbf{u}) = \nabla \cdot (\mu \cdot \text{grad} v) - \frac{\partial p}{\partial y} + S_v \qquad \text{Eqn. 3}$$

$$\frac{\partial (\rho w)}{\partial t} + \nabla \cdot (\rho w \mathbf{u}) = \nabla \cdot (\mu \cdot \text{grad} w) - \frac{\partial p}{\partial z} + S_w \qquad \text{Eqn. 4}$$

Energy conservation equation:

$$\frac{\partial (\rho T)}{\partial t} + \nabla \cdot (\rho \mathbf{u} T) = \nabla \cdot \left(\frac{k}{c_p} \text{grad} T \right) + S_T \qquad \text{Eqn. 5}$$

where ρ is the density; t, the time; $\mathbf{u}$, the velocity vector; u, v and w, the velocity components on x, y and z direction, respectively; μ, the dynamic viscosity of liquid metal; p, the pressure; c_p, the specific heat; k, the thermal conductivity; T, the temperature; and S, the source item.

Basic governing equation of solidification simulation is based on the Fourier heat conduction equation, which is given below[18]:

$$\rho c_p \frac{\partial T}{\partial t} = \nabla^2 \cdot (kT) + \dot{Q} \qquad \text{Eqn. 6}$$

where $\dot{Q}$ is the source item.

The software employs the finite volume approach to convert the differential equations into algebraic ones and solves them on rectangular grids.

Initial and Boundary Conditions

The casting alloy was A356, with a solidus temperature of 542 °C (1008 °F), a liquidus temperature of 613 °C (1135 °F) and a latent heat of 430.52 kJ/kg. H13 steel was applied for the top and bottom die. GJS500-7 ductile iron was used for the side die, and ceramic pipe was used for the riser tube. The properties of all materials are defined in the MAGMA Database.

The initial temperature of A356 was 685.0 °C (1265 °F). The initial temperatures of all dies were 350 °C (662 °F).

The initial thickness of coating on the dies was about 45–60 μm, and the coating became thinner gradually and was re-sprayed once every 12 h. The heat transfer coefficient (HTC) between casting and die was a function of temperature, as shown in Figure 10. The HTC between dies was constant, 800.0 W/m^2 K. The cooling spots included water cooling and air cooling. The pressure of cooling water was about 0.25–0.3 MPa, and the pressure of cooling air was about 0.6 MPa. The HTC of water cooling was 6000.0 W/m^2 K, and the HTC of air cooling was 600.0 W/m^2 K. The HTC between casting and insulation material was 5.0 W/m^2 K when insulation material was employed.

Simulation Model

Simulation model was established based on computer-aided design (CAD) models of casting and dies, as shown in Figure 11. Numerical simulation was implemented, and it included 10 cycles to obtain heat balance of dies. Moreover, 28 key locations were defined to understand whether sequential solidification was achieved, as shown in Figure 12. P1–P13 were located on the maximum section of big spoke, while P′1–P′15 were located on the maximum section of small spoke.

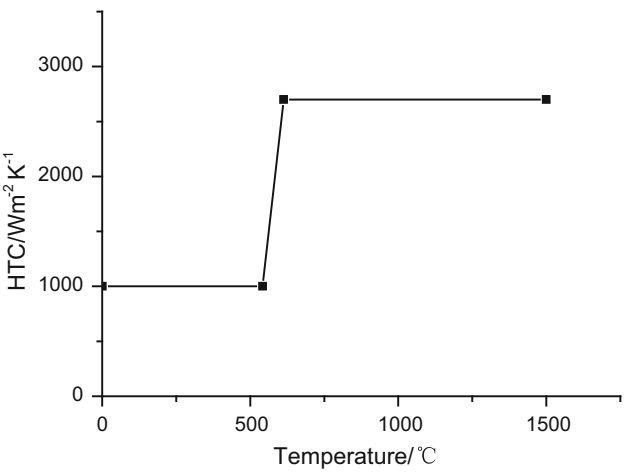

Figure 10. HTC between casting and dies.

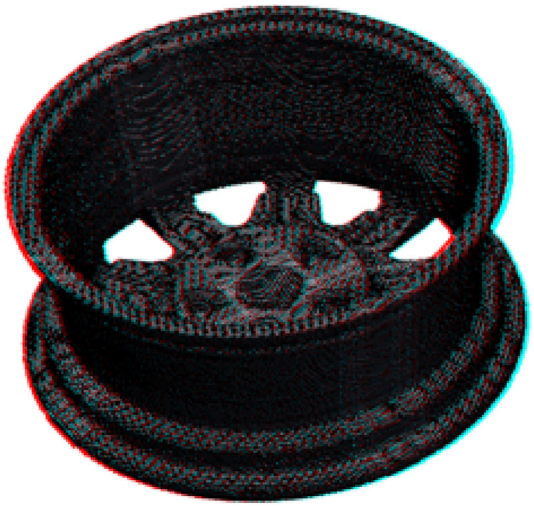

Figure 11. Simulation model of wheel.

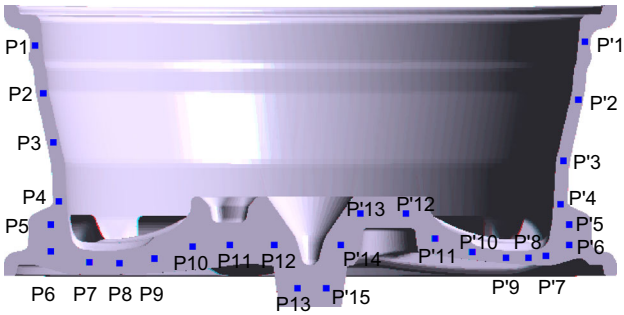

Figure 12. Key locations on section.

Simulation Results and Discussion

Temperature Curves

Measured temperature curves could be obtained according to the experiments. Meanwhile, calculated temperatures could be gained from simulation results, and the curves are illustrated in Figures 13 and 14. The maximum absolute errors and maximum relative errors between measurement and calculation were 10.85 °C and 2.21 % at TC1, and 11.55 °C and 2.31 % at TC2, respectively. It is obvious that the simulation model was rational and simulation accuracy can be guaranteed.

Porosity Contours

Porosity contours are shown in Figure 15, included microporosity, macroporosity and total porosity. It was well known that there were no microporosity defects from Figure 15a, but macroporosity defects occurred in the junctions from Figure 15b, c, and the severity of porosity was more serious in the small spokes than in the big ones. These porosity contours were basically identical with the experimental results shown in Figure 9.

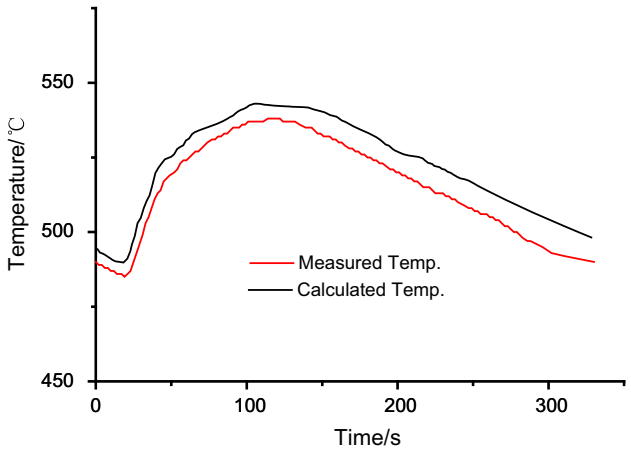

Figure 13. Temperature curves at TC1.

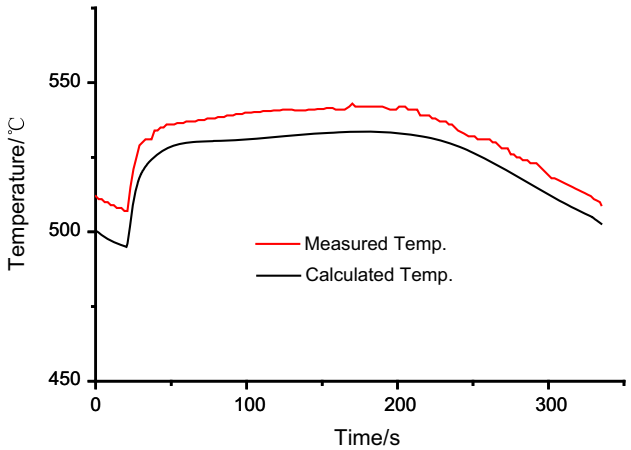

Figure 14. Temperature curves at TC2.

Solidification Time Contours

Different solidification time contours are given in Figure 16a–c. The "FSTime" criterion displays the time that elapses until 30 % of the melt have solidified at the corresponding location. The "Liquidus to Solidus" criterion displays the time that the individual regions of the casting need to cool down from liquidus to solidus temperature. The "Solidification Time" criterion shows the time from the start of the solidification to the time when the temperature falls below the solidus temperature. Moreover, the solidification time curves of different stages are illustrated in Figure 17 for P1–P13 and Figure 18 for P′1–P′15, and some values are listed in Tables 2 and 3.

Figure 17 and Table 2 comprehensively show that according to the "FSTime" curve, the time became longer from P1 to P6, then the time became shorter at P7 and P8, and the time difference between P6 and P8 was 10.4 s. Similarly, according to the "Liquidus to Solidus" curve, the TD between P4 and P6 was 3.6 s. It indicated that feeding paths would be cut off prematurely and hot spots

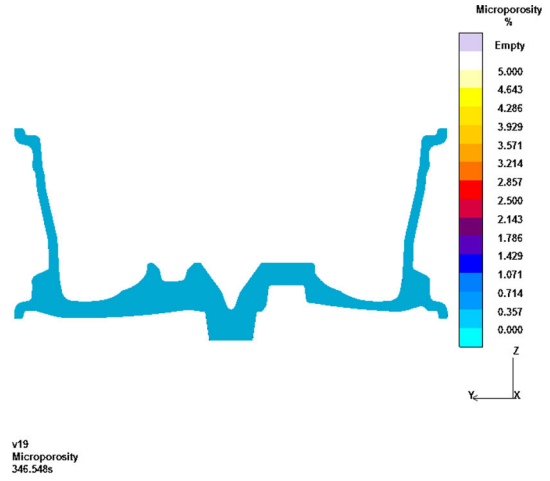

(a)

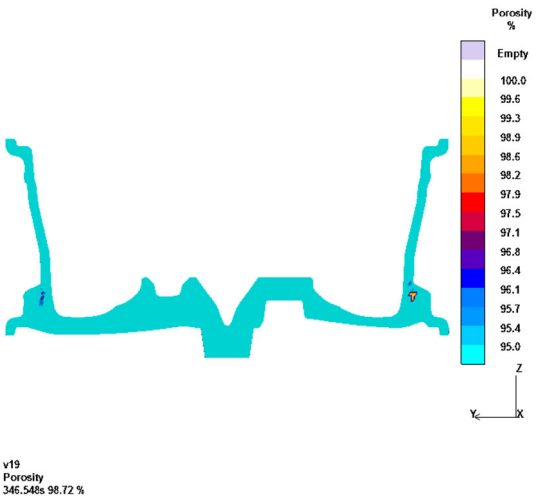

(b)

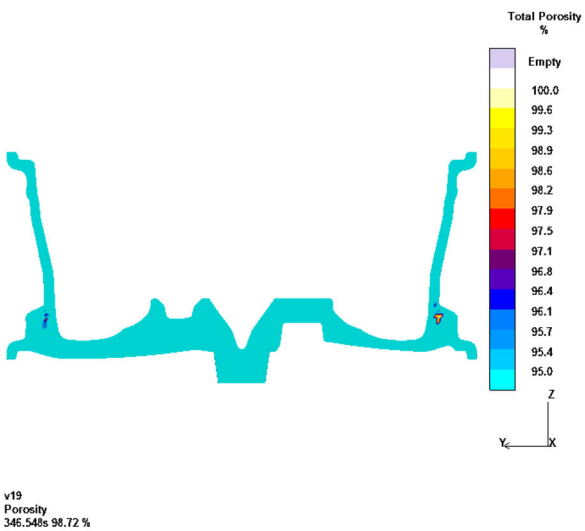

(c)

Figure 15. Porosity contours. (a) Microporosity, (b) macroporosity, (c) total porosity.

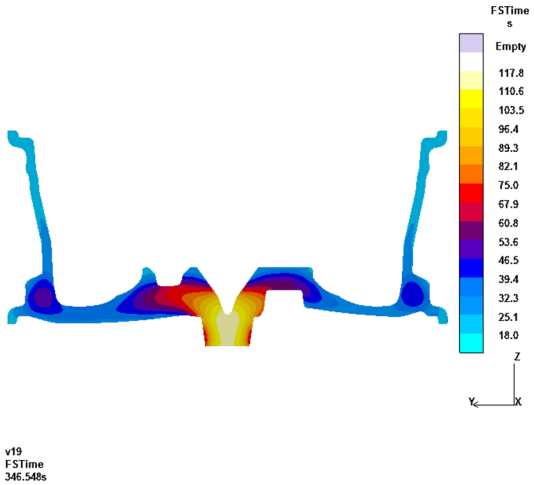

(a)

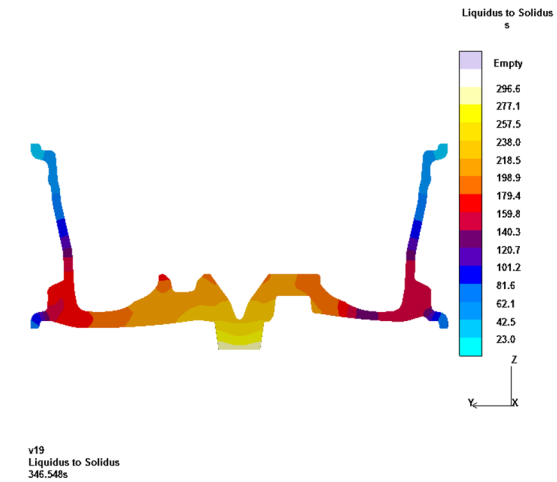

(b)

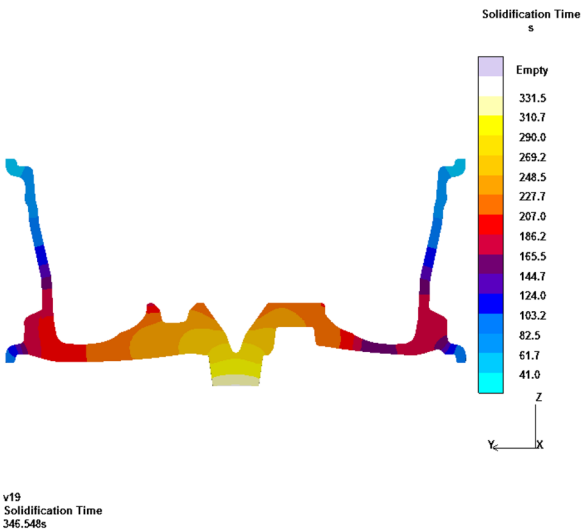

(c)

Figure 16. Different solidification time contours. (a) 30 % fraction solid time, (b) liquidus to solidus time, (c) solidification time.

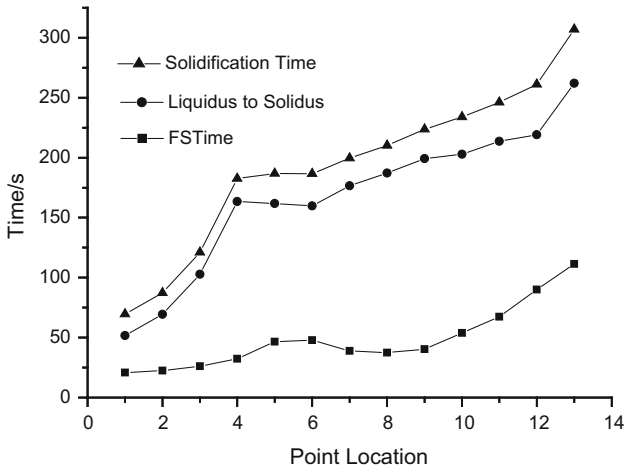

Figure 17. Different solidification time curves at P1–P13.

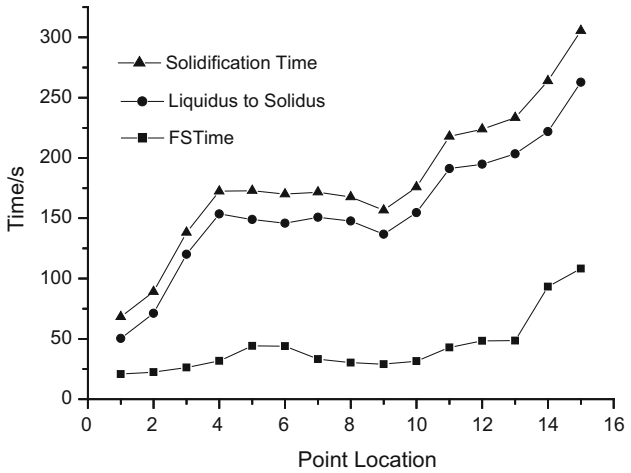

Figure 18. Different solidification time curves at P′1–P′15.

would be formed at location P6, so sequential solidification was unable to be realized completely and some porosity defects would be formed in the junctions. However, compared to the experimental results in Figure 9 and X-ray inspection results, the porosity was about grade 2 and it could be acceptable.

Figure 18 and Table 3 show that the time difference between P′5 and P′9 was 15.1 s for the "FSTime" curve. The time difference between P′4 and P′9 was 16.9 s for the "Liquidus to Solidus" curve. It showed that the feeding paths would be cut off more early and bigger hot spots would be formed at location P′5 than P6. The experimental results indicated the porosity was grade 4 and it was unsatisfied with the technical requirements. So the LPDC process, especially cooling process, should be improved to avoid macroporosity defects which were greater than grade 3.

Improvement and Verification

Improved Cooling Process

Some insulation spots were designed on the top and bottom die based on above simulation results to prolong solidification time and keep the feeding paths working at the corresponding location, as shown in Figures 19 and 20. The times the cooling spots were switched on and off were modified and are listed in Table 4.

Porosity Contours

Simulation was implemented again, and contours with porosity defects are given in Figure 21. It can be known there were no microporosity defects. The severity of macroporosity defects was improved, and the defects were approximately grade 2 compared to the results in Figure 15. The simulation results indicated the casting might be qualified.

Solidification Time Contours

Solidification time contours of different stages are illustrated in Figure 22. The corresponding curves are shown in

Table 2. Different Solidification Time

Location	P4	P5	P6	P7	P8	P9
FSTime (s)	32.2	46.5	47.9	38.8	37.5	40.3
Liquidus to solidus (s)	163.4	161.8	159.8	176.6	187.1	199.2
Solidification time (s)	182.7	186.7	186.6	199.6	210.1	223.7

Table 3. Different Solidification Time

Location	P′4	P′5	P′6	P′7	P′8	P′9	P′10
FSTime (s)	31.8	44.2	43.9	33.2	30.2	29.1	31.6
Liquidus to solidus (s)	153.6	149.0	145.9	150.8	147.7	136.7	154.6
Solidification time (s)	172.31	173.0	170.0	171.6	167.7	156.6	175.7

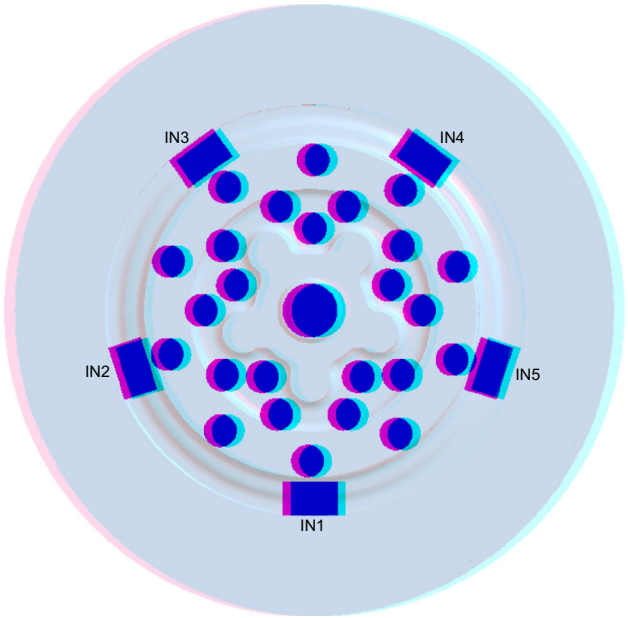

Figure 19. Cooling and insulation spots on top die.

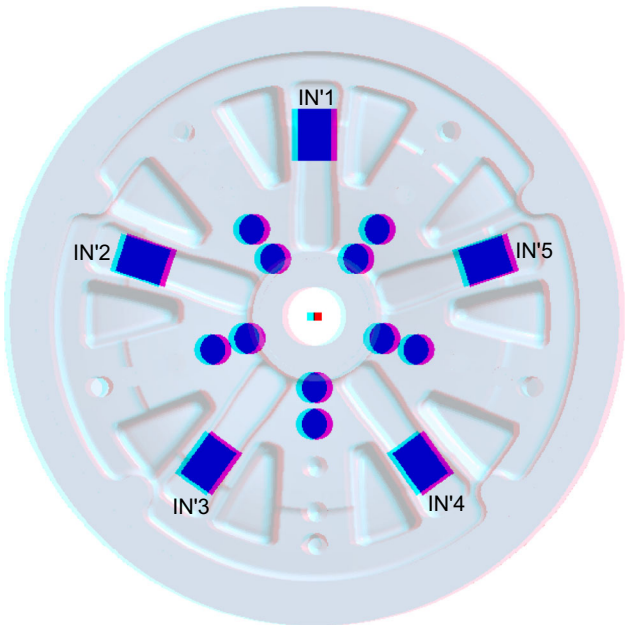

Figure 20. Cooling and insulation spots on bottom die.

Table 4. Time of Switch On/Off of All Cooling Spots

No. of cooling spot	Time of switch on (s)	Time of switch off (s)
C1	170	250
C2–C6	140	220
C7–C16	130	280
C17–C26	190	220
C27–C31	110	280
C32–C36	200	280

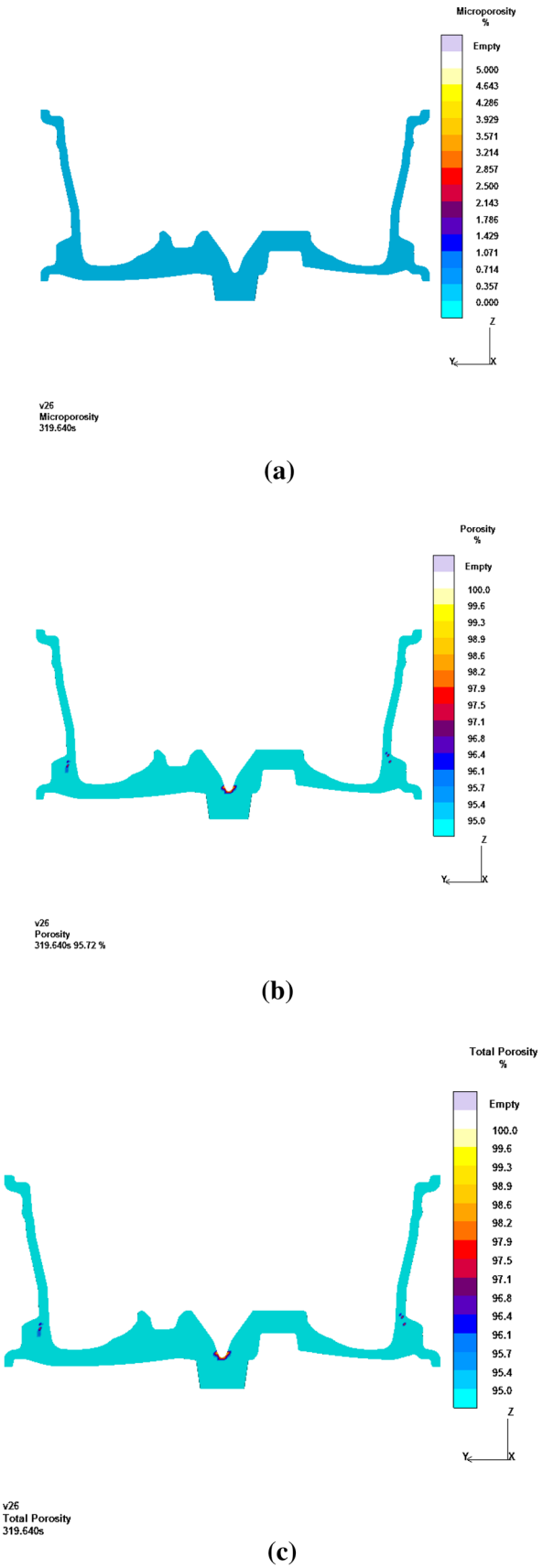

Figure 21. Porosity defects contours. (a) Microporosity defects, (b) macroporosity defects, (c) total porosity defects.

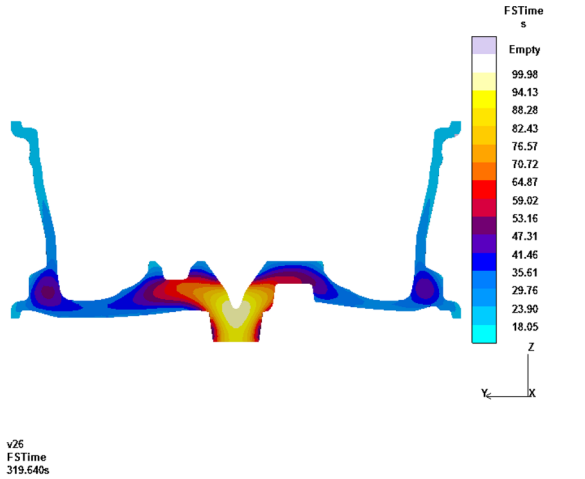

(a)

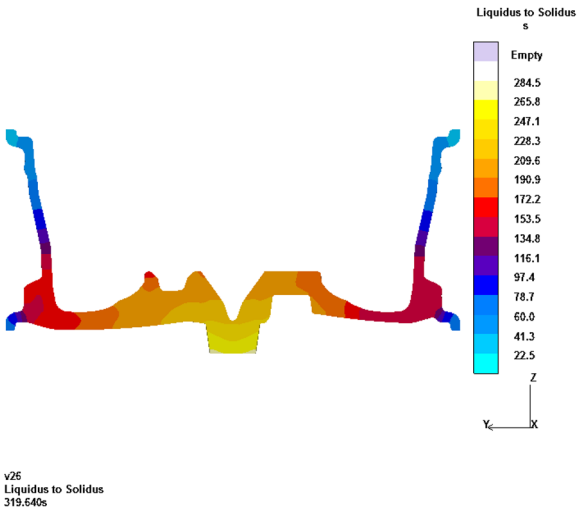

(b)

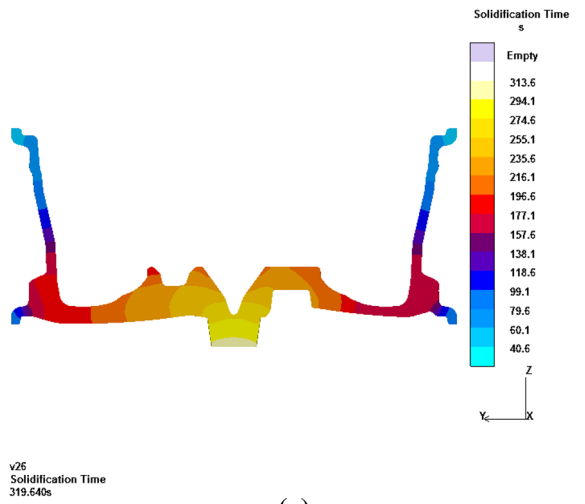

(c)

Figure 22. Different solidification time contours. (a) 30 % fraction solid time, (b) liquidus to solidus time, (c) solidification time.

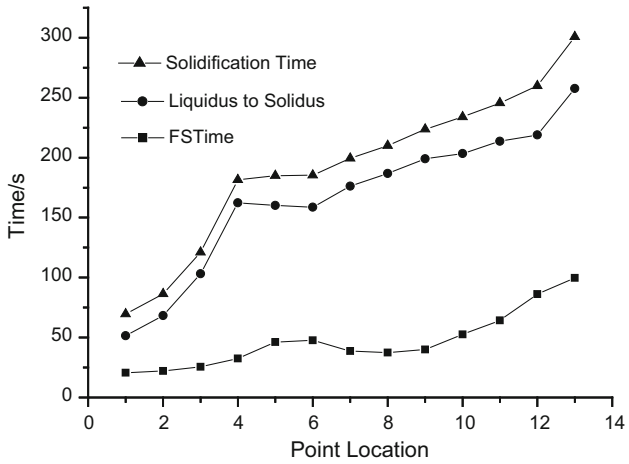

Figure 23. Different solidification time curves at P1–P13.

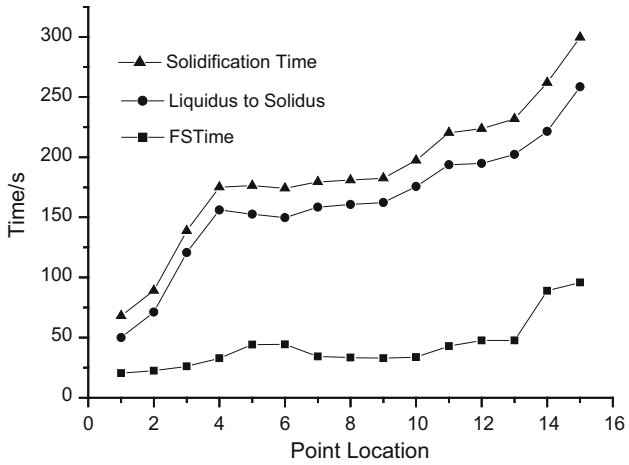

Figure 24. Different solidification time curves at P′1–P′15.

Figure 23 for P1–P13 and Figure 24 for P′1–P′15, and some values are listed in Tables 5 and 6.

Figure 23 and Table 5 show that the time difference between P6 and P8 was 10.2 s for the "FSTime" curve, while the time difference between P4 and P6 was 3.6 s for the "Liquidus to Solidus" curve. It was similar to the results shown in Figure 17 and Table 2 which showed the porosity defects can be acceptable.

Figure 24 and Table 6 show that the TD between P′6 and P′9 was 11.4 s for the "FSTime" curve, and the time difference between P′4 and P′9 was 6.4 s for the "Liquidus to Solidus" curve. Compared to Figure 18 and Table 3, the time difference shortened from 15.1 to 11.4 s for "FSTime" and from 16.9 to 6.4 s for "Liquidus to Solidus." It demonstrated that the insulation spots had a good effect on prolonging the solidification time at the location with thin wall thickness, keeping the feeding paths cutoff and decreasing the size of hot spots and corresponding porosity defects.

Table 5. Different Solidification Time

Location	P4	P5	P6	P7	P8	P9
FSTime (s)	32.5	46.2	47.7	38.8	37.5	40.0
Liquidus to solidus (s)	162.2	160.2	158.6	176.2	186.8	199.1
Solidification time (s)	181.6	185.0	185.4	199.4	210.0	223.7

Table 6. Different Solidification Time

Location	P′4	P′5	P′6	P′7	P′8	P′9	P′10
FSTime (s)	32.8	44.2	44.3	34.3	33.5	32.9	33.9
Liquidus to solidus (s)	156.1	152.7	149.7	158.4	160.8	162.3	175.7
Solidification time (s)	175.1	176.4	174.2	179.4	181.0	182.6	197.4

Figure 25. No macroporosity.

Experimental Verification

LPDC experiments were conducted to verify the feasibility of improved cooling and insulation process.

The experimental wheel castings were detected by X-ray inspection equipment, and some obscure porosity defects were found in the junctions, which were about grade 2. It indicated the defects could be acceptable. Consequently, the casting was cut and the section is shown in Figure 25. There were no macroporosity defects in the junctions. Therefore, the experimental results verified the improved cooling and insulation process was feasible and it could guarantee the casting quality.

Conclusions

1. Simulation model was established for the LPDC experiments. The calculated temperatures were basically in good agreement with the measured ones which indicated the initial/boundary conditions were defined correctly and the simulation accuracy can be guaranteed.
2. Solidification times of different stages demonstrated it was very difficult to promote sequential solidification completely and eliminate hot spots entirely for the complex wheel casting. However, simulation technology can be used effectively to improve the cooling and insulation process which could prevent the feeding paths cutoff prematurely and decrease the size of hot spots and corresponding porosity defects.
3. It was very important to determine the quantitative relationship between simulation results and X-ray inspection standard for porosity defects. Some experiments and X-ray inspection results should be conducted to compare with porosity contours so as to determine the approximately corresponding relationship.

REFERENCES

1. M. Merlin, G. Timelli, F. Bonollo, F. Bonollo, G.L. Garagnani, Impact behavior of A356 alloy for low-pressure die casting automotive wheels. J. Mater. Process. Technol. **209**, 1060–1073 (2009)
2. J.H. Kuo, F.L. Hsu, W.S. Hwang, Development of an interactive simulation system for the determination of the pressure-time relationship during the filling in a low pressure casting process. Sci. Technol. Adv. Mater. **2**, 131–145 (2001)
3. J.A. Hines, Determination of interfacial heat-transfer boundary conditions in an aluminum low-pressure permanent mold test casting. Metall. Mater. Trans. B **35B**(4), 299–311 (2004)
4. B. Zhang, S.L. Cockcroft, D.M. Maijer, J.D. Zhu, A.B. Phillion, Casting defects in low-pressure die-cast aluminum alloy wheels. JOM **57**(11), 36–43 (2005)
5. A.E. Miller, D.M. Maijer, Investigation of erosive–corrosive wear in the low pressure die casting of

aluminum A356. Mater. Sci. Eng. A **435–436**, 100–111 (2006)
6. B. Zhang, D.M. Maijer, S.L. Cockcroft, Development of a 3-D thermal model of the low-pressure die-cast (LPDC) process of A356 aluminum alloy wheels. Mater. Sci. Eng., A **464**, 295–305 (2007)
7. X. Zhang, S. Tong, L. Xu, S. Yan, Optimization of low-pressure die casting process with soft computing, in *Proceedings of the 2007 IEEE International Conference on Mechatronics and Automation,* Harbin, China, pp. 619–623 (2007)
8. D.M. Maijer, W.S. Owen, R.A. Vetter, An investigation of predictive control for aluminum wheel casting via a virtual process model. J. Mater. Process. Technol. **209**, 1965–1979 (2009)
9. G. Mi, X. Liu, K. Wang, H. Fu, Numerical simulation of low pressure die-casting aluminum wheel. China Foundry **6**(1), 48–52 (2009)
10. P.W. Cleary, Extension of SPH to predict feeding, freezing and defect creation in low pressure die casting. Appl. Math. Model. **34**, 3189–3201 (2010)
11. X.M. Shi, D. Maijer, G.A. Dumont, Determination of optimal location to monitor temperature in low pressure die casting process. Mater. Sci. Technol. **27**(6), 1073–1083 (2011)
12. C. Reilly, J. Duan, L. Yao, D.M. Maijer, S.L. Cockcroft, Process modeling of low-pressure die casting of aluminum alloy automotive wheels. JOM **65**(9), 1111–1121 (2013)
13. G. Nicoletto, G. Anzelotti, R. Konecna, X-ray computed tomography vs. metallography for pore sizing and fatigue of cast Al-alloys. Procedia Eng. **2**, 547–554 (2010)
14. M.A. Islam, Z.N. Farhat, The influence of porosity and hot isostatic pressing treatment on wear characteristics of cast and p/m aluminum alloys. Wear **271**, 1594–1601 (2011)
15. N. Vanderesse, E. Maire, A. Chabod, J.Y. Buffiere, Microtomographic study and finite element analysis of the porosity harmfulness in a cast aluminium alloy. Int. J. Fatigue **33**, 1514–1525 (2011)
16. Y. Wang, D. Li, Y. Peng, X. Zeng, Numerical simulation of low pressure die casting of magnesium wheel. Int. J. Adv. Manuf. Technol. **32**, 257–264 (2007)
17. H.K. Versteeg, W. Malalasekera, *An Introduction to Computational Fluid Dynamics: The Finite Volume Method* (Wiley, New York, 1995)
18. D.M. Stefanescu, G. Upadhya, D. Bandyopanhyay, Heat transfer-solidification kinetics modeling of solidification of castings. Metall. Trans. A **4**(21A), 997–1005 (1990)

Technical Review and Discussion

Effect of Cooling Process on Porosity in the Aluminum Alloy Automotive Wheel During Low Pressure Die Casting

Dashan Sui, Zhenshan Cui; Shanghai Jiao Tong University, Shanghai, China

Rong Wang, Shengfei Hao; Dare Wheel Manufacturing Co., Ltd., Zhenjiang, Jiangsu, China

Qingyou Han; Purdue University, West Lafayette, IN, USA

Reviewers: It would be helpful to have more description about what kind of thermocouples with what response time etc. were used, as it can impact the actual temperature versus time results.

Authors: *K-type thermocouples were used to measure the temperature of dies, with a response time of 0.5 s.*

Reviewers: More data collection and simulation correlation are needed. Correlation should consider collecting data over several shots and simulating those conditions along with analyzing the castings for each shot.

Authors: *Actually, 100 wheels were produced according to scheme No. 3. The data collected for each shot were similar after 20th cycle. We reported the stable data in the paper.*